CHEMISTRY OF MATERIALS

Article

pubs.acs.org/cm

Stable Interface Formation between TiS_2 and $LiBH_4$ in Bulk-Type All-Solid-State Lithium Batteries

Atsushi Unemoto,*[,†] Tamio Ikeshoji,[†,‡] Syun Yasaku,[‡] Motoaki Matsuo,[‡] Vitalie Stavila,[§] Terrence J. Udovic,[∥] and Shin-ichi Orimo[†,‡]

[†]WPI−Advanced Institute for Materials Research (WPI−AIMR), Tohoku University, 2-1-1 Katahira, Aoba-ku, Sendai 980-8577, Japan

[‡]Institute for Materials Research, Tohoku University, 2-1-1 Katahira, Aoba-ku, Sendai 980-8577, Japan

[§]Energy Nanomaterials, Sandia National Laboratories, Livermore, California 94551, United States

[∥]NIST Center for Neutron Research, National Institute of Standards and Technology, Gaithersburg, Maryland 20899-6102, United States

Supporting Information

ABSTRACT: In this study, we assembled a bulk-type all-solid-state battery comprised of a TiS_2 positive electrode, $LiBH_4$ electrolyte, and Li negative electrode. Our battery retained high capacity over 300 discharge−charge cycles when operated at 393 K and 0.2 C. The second discharge capacity was as high as 205 mAh g^{-1}, corresponding to a TiS_2 utilization ratio of 85%. The 300th discharge capacity remained as high as 180 mAh g^{-1} with nearly 100% Coulombic efficiency from the second cycle. Negligible impact of the exposure of $LiBH_4$ to atmospheric-pressure oxygen on battery cycle life was also confirmed. To investigate the origin of the cycle durability for this bulk-type all-solid-state TiS_2/Li battery, electrochemical measurements, thermogravimetry coupled with gas composition analysis, powder X-ray diffraction measurements, and first-principles molecular dynamics simulations were carried out. Chemical and/or electrochemical oxidation of $LiBH_4$ occurred at the TiS_2 surface at the battery operating temperature of 393 K and/or during the initial charge. During this oxidation reaction of $LiBH_4$ with hydrogen (H_2) release just beneath the TiS_2 surface, a third phase, likely including $Li_2B_{12}H_{12}$, precipitated at the interface between $LiBH_4$ and TiS_2. $Li_2B_{12}H_{12}$ has a lithium ionic conductivity of $\log(\sigma / S\ cm^{-1}) = -4.4$, charge transfer reactivity with Li electrodes, and superior oxidative stability to $LiBH_4$, and thereby can act as a stable interface that enables numerous discharge−charge cycles. Our results strongly suggest that the creation of such a stable interfacial layer is due to the propensity of forming highly stable, hydrogen-deficient polyhydro-*closo*-polyborates such as $Li_2B_{12}H_{12}$, which are thermodynamically available in the ternary Li−B−H system.

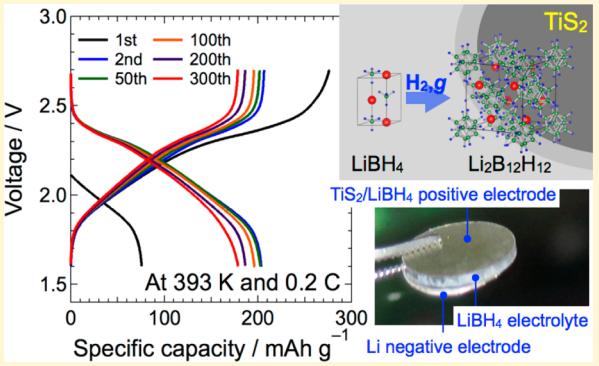

1. INTRODUCTION

The all-solid-state battery, which consists of solid-state components (anode, cathode, and electrolyte), is considered as one of the most promising candidates for future-generation energy storage.[1,2] This is because the solid-state electrolytes used in these batteries expand the choice of the electrodes incorporated into the battery and allow for flexible battery design, i.e., bipolar stacking structure, which is advantageous in terms of both energy and power densities.[3] In addition, it overcomes the concerns related to safety, including Li dendrite formation and leakage and vaporization of liquid electrolytes, currently problematic for the commercial lithium-ion batteries that use organic liquid solvents.[1,2] Thus, the all-solid-state battery would be advantageous for utilization in large-scale applications including stationary uses for load leveling, electric vehicles, and so forth.

Research and development efforts of solid-state electrolytes for all-solid-state batteries have so far been focused mainly on oxides and sulfides, some of which have fast ionic conductivities.[4] Besides favorable conductivities, it is also crucial for durable, high-performance battery operation to possess an interface with both high electrochemical and chemical stabilities. It has been suggested that the mutual diffusion of constituent elements across the interface between the positive electrode and electrolyte increases the interface resistance, resulting in capacity fading.[5,6] In such systems, introduction of a protective layer is effective for enhancing the cycle life. Thus, the overall success of the all-solid-state battery relies not only on realizing the fast ionic conduction of solid-

Received: June 4, 2015
Revised: July 14, 2015
Published: July 14, 2015

DOI: 10.1021/acs.chemmater.5b02110
Chem. Mater. 2015, 27, 5407−5416

state electrolytes but also introducing a stable interface between the electrode and electrolyte.

Metal hydrides are considered as promising functional materials in several areas of advanced energy storage such as (i) high-density solid-state hydrogen storage (e.g., $LiBH_4$ contains the equivalent of 18.5 mass % H_2 and 12.4 kg H_2 m^{-3}),[7,8] (ii) high-capacity lithium storage for use as negative electrodes in lithium rechargeable batteries [e.g., MgH_2 (2038 mAh g^{-1} and 2878 Ah l^{-1})[9−13] and Mg_2FeH_6 (1456 mAh g^{-1} and 3995 Ah l^{-1})[14,15] both having higher specific capacities than the conventional graphite negative electrode (372 mAh g^{-1} and 840 Ah l^{-1})],[16] and (iii) fast ionic conduction in complex metal hydrides for use as electrolytes in all-solid-state batteries.[17−19]

In the latter area, complex metal hydrides have recently emerged as an alternative type of solid-state electrolyte to sulfides and oxides.[17−19] The high reducing ability of this class of materials was assumed to promote decomposition reactions with highly oxidative positive electrode materials. Because of this possibility, less research has been done to use this type of electrolyte in solid-state batteries, even though some of them exhibit fast lithium ionic conductivity. Complex hydrides are expressed by the general formula $M(M'H_n)$, where M is the metal cation and $M'H_n$ is the complex anion (e.g., $[BH_4]^-$, $[NH_2]^-$, $[AlH_4]^-$).[8] For instance, $LiBH_4$ has an orthorhombic structure at room temperature but undergoes a phase transition to a hexagonal structure at elevated temperatures around 390 K. The high-temperature phase of $LiBH_4$ exhibits a high lithium ionic conductivity that exceeds $\log(\sigma/S\ cm^{-1}) = -2.7$ at temperatures above the phase transition.[17−19] Partial substitution of the $[BH_4]^-$ anion by the iodide anion, I^-, stabilizes the hexagonal phase of $LiBH_4$ at reduced temperatures. As a result, the solid-solution, $Li_4(BH_4)_3I$, exhibits a lithium ionic conductivity of $\log(\sigma / S\ cm^{-1}) = -4.7$ at room temperature.[20]

Researchers recently tested the performance of all-solid-state batteries that use complex hydride-based electrolytes.[19,21−25] Although the high reducing ability of this class of materials allowed using a lithium negative electrode for battery assembly,[17−25] it invited unfavorable decomposition of a high-voltage electrode such as $LiCoO_2$ (3.9 V vs Li/Li^+)[26] and thereby destabilized the battery operation. This issue was overcome by introducing a thin protective layer of a solid-state electrolyte such as Li_3PO_4 between $LiCoO_2$ and $LiBH_4$ electrolytes to avoid direct contact between them. Indeed, 30 charge−discharge cycles were successfully demonstrated with discharge capacities of ∼90 mAh g^{-1}, corresponding to a $LiCoO_2$ utilization ratio of 65% over the battery test.[21,22]

When a positive electrode with low redox potential is incorporated into the battery assembly, such a protection layer is unnecessary. Sveinbjörnsson and co-workers assembled an all-solid-state battery using a $Li_4Ti_5O_{12}$ positive electrode with a redox potential of approximately 1.55 V (vs Li/Li^+), a Li negative electrode, and a $LiBH_4$−LiI solid-solution electrolyte and operated it at 333 K. Without placing any protection layer between $Li_4Ti_5O_{12}$ and $LiBH_4$−LiI, the authors realized a discharge capacity of more than 110 mAh g^{-1} (65% $Li_4Ti_5O_{12}$ utilization ratio) in the initial 10 discharge−charge cycles.[23]

Our research group also succeeded in constructing a "bulk-type" all-solid-state battery incorporating particulate electrode and electrolyte layers.[27] Typically, the electrode layer in bulk-type batteries developed thus far is a composite of active material and electrolyte particles with a thickness of the order of or larger than 100 μm. Hence, this type of battery stores a high quantity of active material in the electrode layer and is thereby advantageous in terms of overall energy density compared to solid-state batteries that have thin electrode layers with thicknesses of a few micrometers or less.

Our bulk-type all-solid-state battery containing a TiS_2 positive electrode and $LiBH_4$ electrolyte exhibited a discharge capacity of 200 mAh g^{-1} (83% TiS_2 utilization ratio) during 30 cycles when operated at 393 K. The battery operating temperature could be lowered below 393 K by the use of a $Li_4(BH_4)_3I$ electrolyte.[19] Considering the high compatibility to the lowest-voltage lithium negative electrode with the complex hydride electrolyte, even the positive electrode material with low redox potential can be used to give relatively high voltage. From this point of view, we recently incorporated a high-capacity elemental sulfur positive electrode that possessed a theoretical capacity of 1672 mAh g^{-1} with a redox potential of ∼2.2 V.[28] The battery exhibited a discharge capacity that exceeded 700 mAh g^{-1} over 45 cycles at 393 K.[24] Due to their fast-ionic conduction and successful incorporation into solid-state batteries, complex hydrides are now recognized as a novel solid-state electrolyte family worthy of further study for use in rechargeable batteries.[19]

The success of stable battery operation relies on introducing a robust interface that hinders the side reaction and mutual diffusion of constituent elements between the electrode-active material and the solid-state electrolyte. In this study, we propose a unique formation mechanism of the stable interface between TiS_2 and $LiBH_4$. This interface formed as a result of the solid-state reaction that accompanied gas desorption from $LiBH_4$ just beneath the TiS_2 surface, allowing for stable operation over numerous discharge−charge cycles. Moreover, the cycle life was not affected by the exposure of the $LiBH_4$ electrolyte to high-pressure oxygen. Such a durable interface, similar to the solid electrolyte interphase (SEI) typically forming between the nonaqueous electrolyte and graphite negative electrode,[29] is made possible by the formation of highly stable, H-deficient, complex-hydride byproducts of $LiBH_4$.

2. EXPERIMENTAL SECTION

2.1. Battery Test. Commercially available powders of TiS_2 (99.9%, Sigma-Aldrich)[30] and $LiBH_4$ (≥95%, Sigma-Aldrich) were used as received for the positive electrode active material and the solid-state electrolyte, respectively. The TiS_2 and $LiBH_4$ powders were weighed in a 2:3 mass ratio and mixed by an agate mortar in an agate pestle. The resultant mixture was used as the composite positive electrode. First, 20 mg of $LiBH_4$ powder was placed into an 8-mm-diameter die and uniaxially pressed at 60 MPa. Subsequently, 6 mg of the composite positive electrode powder was transferred onto the pressed electrolyte still present in the die and uniaxially pressed at 240 MPa to obtain one single pellet comprised of the composite positive electrode and the electrolyte layers. Li foil (Honjo Metal Co., Ltd.) was used as a negative electrode and placed opposite of the positive electrode, as in the photo shown in Figure 1. The assembled bulk-type all-solid-state TiS_2/Li battery was placed in a stainless steel electrochemical cell with an 8-mm-diameter Teflon guide as schematically illustrated elsewhere.[24] The battery assembly was carried out in an Ar-filled glovebox. The electrochemical cell was also filled with Ar. The battery test was carried out with 0.2 C charge rate, corresponding to 230 $\mu A\ cm^{-2}$, in the voltage range of 1.6−2.7 V at 393 K.

2.2. Electrochemical Measurements. AC impedance measurements with the two-probe technique were carried out by using Li- and Au-symmetric cells using the $Li_2B_{12}H_{12}$ electrolyte at 393 K. The synthetic route[31] and the crystal structure analysis[32] of $Li_2B_{12}H_{12}$ are described elsewhere. The powders of $Li_2B_{12}H_{12}$ were placed in an 8-

DOI: 10.1021/acs.chemmater.5b02110
Chem. Mater. 2015, 27, 5407−5416

mm-diameter die and then uniaxially pressed at 240 MPa. The resultant compacts were sandwiched by Li and Au electrodes and placed in a stainless steel electrochemical cell similar to the battery test as described above. The input voltage perturbation and frequency range were 0.1 V and 1 M−10 Hz, respectively. AC impedance measurements were also carried out for the bulk-type all-solid-state TiS_2/Li battery. The measurements were performed just before the battery test and after the initial discharge and initial charge at 393 K. The input voltage perturbation and frequency range were 10 mV and 1 M−10 mHz, respectively. The open circuit potential (OCP) of the Li_xTiS_2 as a function of lithium concentration, x, was evaluated by means of the Coulombic titration technique at 393 K. The electrochemical cell with the bulk-type all-solid-state TiS_2/Li battery configuration as described above was employed. To avoid the effects of self-discharge before the measurement and irreversible oxidation during charging, two discharge−charge cycles were carried out at 0.1 C. After the second full charge, the discharge current, corresponding to 0.1 C, was applied for 15 min, and subsequently, the electrochemical cell was left in an open circuit for 3 h for equilibration to obtain OCP. The procedure was repeated until the cell voltage under current flow reached down to 1.5 V.

2.3. Thermogravimetry Coupled with Gas Composition Analysis. The mixed TiS_2 and $LiBH_4$ compact that had the same composition as the composite positive electrode for the bulk-type all-solid-state TiS_2/Li battery was subjected to thermogravimetry (TG) coupled with gas composition analyses by a quadrupole mass spectrometer (QMS) at elevated temperatures up to 400 K raised by 5 K min^{-1} in He flow. The measurements were carried out for two heating runs.

2.4. X-ray Diffraction Measurements. The reactivity between TiS_2 and Li−B−H complex hydrides including $LiBH_4$ and $Li_2B_{12}H_{12}$ was investigated by powder X-ray diffraction (XRD) measurements with Cu Kα radiation (X'pert PRO, PANalytical) at room temperature. The powders of TiS_2 and Li−B−H complex hydrides were separately weighed in the desired ratios and then uniaxially pressed at 240 MPa. The resultant compacts were annealed at 393 K for 2 h in an Ar-filled environment. After annealing, the compacts were ground by an agate mortar in an agate pestle. Then, the XRD patterns were collected for the resultant powder that was placed into a glass capillary with 0.5 mm inner diameter.

2.5. First-Principles Molecular Dynamics Simulation. We used density functional theory (DFT) with plane-wave basis sets under the periodic boundary condition. Ultrasoft pseudopotentials[33] were used for inner core electrons. A Perdew−Burke−Ernzerhof (PBE) functional[34] was used as the exchange correlation with a generalized gradient approximation (GGA). Cutoff energies of 25 Ry (1 Ry = 13.606 eV) were used for wave functional and 225 Ry for electron density. In the molecular dynamics calculation, we replaced the hydrogen mass with the deuterium mass to make a large time step of 1.2 fs possible for time integration of the Newtonian equations of motion. The temperature was kept constant by velocity scaling. The simulation time was about 1−2 ps. The first-principles molecular dynamics (FPMD) calculation was performed using "Simulation Tool for Atom Technology (STATE)".[35]

3. RESULTS AND DISCUSSION

3.1. Battery Performance. In our bulk-type all-solid-state battery configuration, the TiS_2 and $LiBH_4$ composite was used for the positive electrode layer. $LiBH_4$ and Li were used for the electrolyte and the negative electrode, respectively. Owing to the highly deformable nature of $LiBH_4$, uniaxial pressing at 240 MPa and room temperature was sufficient to obtain the compact consisting of the composite positive electrode and the electrolyte, as in the photograph shown in Figure 1.[19] When the TiS_2 and $LiBH_4$ compact was annealed at the battery operating temperature of 393 K, small pores were induced in the $LiBH_4$ phase just beneath the TiS_2 surface. Such pores appeared near the edge-plane of TiS_2 (see microstructure observation results in Supporting Information, Figure S1). Thus, although not proven, one might reasonably postulate that this pore formation is related to the Li intercalation reaction from $LiBH_4$ into TiS_2 and that reaction accompanied the composition variation of the $LiBH_4$ phase. Despite the microstructure change as a result of annealing, the original extensive interfacial contact between $LiBH_4$ and TiS_2, which enables facile charge transfer, remained. Thus, our battery exhibited a high TiS_2 utilization ratio as well as good cycle life, as discussed later. Microstructure characterization of the TiS_2 and $LiBH_4$ composite positive electrode is revealed elsewhere (also see microstructure observation in Supporting Information, Figure S1).[19] Highly deformable $LiBH_4$ also enabled the formation of a tight interface for Li-ion transport between the positive electrode and electrolyte layers.

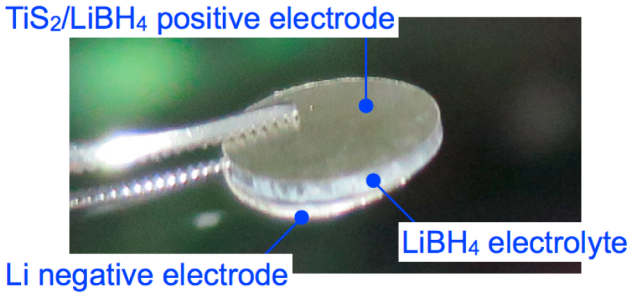

Figure 1. Photograph of the bulk-type all-solid-state TiS_2/Li battery assembled in this study. A part of the Li negative electrode was delaminated for clarity of the battery configuration.

Our bulk-type all-solid-state TiS_2/Li battery retained high capacity over 300 discharge−charge cycles when operated at 393 K and 0.2 C, as shown in Figure 2a. The second discharge capacity was 205 mAh g^{-1}, which corresponds to a TiS_2 utilization ratio of ∼85% (the theoretical capacity is 239 mAh g^{-1} when x in Li_xTiS_2 varies in the range of $0 \le x \le 1$).[36,37] Figure 2b shows the discharge capacity, Coulombic efficiency, and discharge capacity retention ratio to the second discharge as a function of cycle number. Nearly 100% Coulombic efficiency during the numerous cycles suggests that the remarkable side reaction unlikely proceeds any further after the first cycle. Thus, the discharge capacity retention ratio to the second discharge at the 300th remains as high as 88%.

Contrary to the stable battery operation forward from the second discharge, two anomalies appeared in the initial discharge profile: (i) OCP was nearly 2.1 V (vs Li/Li^+) before the initial discharge. This value was smaller than the OCP expected from TiS_2 (2.5 V vs Li/Li^+).[38,39] (ii) A significant difference was observed between the theoretical capacity (239 mAh g^{-1}) and initial discharge capacity (80 mAh g^{-1}). At the second cycle, the discharge capacity was nearly 205 mAh g^{-1}, and the Coulombic efficiency was almost 100%. This suggests that anomalies observed in the initial profiles would be related to the formation of the stable interface that allows for repeated discharge−charge cycles. Thus, we examined the origin of the stable interface formation between TiS_2 and $LiBH_4$ in terms of the electrochemical and chemical reactivity between them.

The electrolyte stability under environmental conditions is of particular importance in the large-scale battery assembling process using a complex hydride electrolyte. Metal borohydrides are easily hydrolyzable, as exemplified by $LiBH_4$, via the reaction $LiBH_4 + 2H_2O \rightarrow LiBO_2 + 4H_2$.[40,41] Thus, $LiBH_4$ is unstable to atmospheric water vapor. In addition, since $LiBH_4$ is

DOI: 10.1021/acs.chemmater.5b02110
Chem. Mater. 2015, 27, 5407−5416

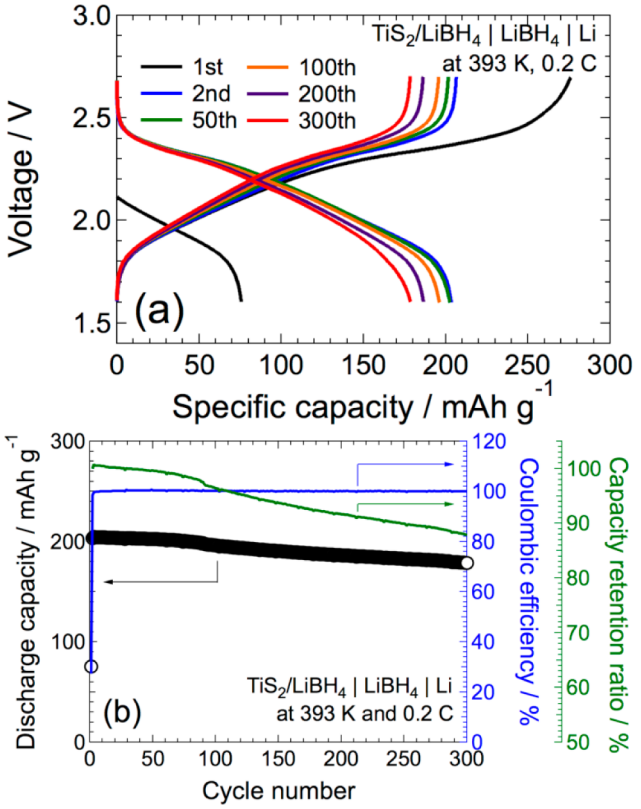

Figure 2. Performance of the bulk-type all-solid-state TiS_2/Li battery operated at 393 K and 0.2 C. (a) Discharge−charge profiles and (b) discharge capacity, Coulombic efficiency (discharge capacity over charge capacity), and discharge capacity retention ratio (to the second discharge capacity). Theoretical capacity of TiS_2 is 239 mAh g^{-1} when x in Li_xTiS_2 varies in the range of $0 \le x \le 1$.[36,37]

a strong reducing agent, it reacts with oxygen under atmospheric conditions to form multicomponent oxides and hydroxides, such as Li_2O and $Li_xB_yO_zH_m$ at the $LiBH_4$ surface.[42] Thus, there might be an argument that the exposure of $LiBH_4$ to atmospheric oxygen would also affect the interface stability between TiS_2 and $LiBH_4$ and thereby battery performance. We carried out the preparation of the bilayer compact consisting of the composite positive electrode and the electrolyte layers in a dry room to avoid the influence from water vapor. Despite the long-term (3 h 20 min) exposure of the powders containing $LiBH_4$ to atmospheric oxygen, our battery exhibited a notably high TiS_2 utilization ratio as well as good cycle life, similar to the battery assembled in an Ar-filled glovebox, as shown in Figure 2. The initial discharge capacity was 190 mAh g^{-1}, and the second one recovered to 205 mAh g^{-1}. The capacity retention ratio at the 50th discharge (to the second discharge) was 96% with nearly 100% Coulombic efficiency (See details on the battery performance and characterization of specimens in Supporting Information, Figures S2 and S3). Since the structure and composition of the $LiBH_4$ surface that may contain Li_2O and $Li_xB_yO_zH_m$ after exposure to oxygen is complicated,[42] further investigation is necessary to better understand the materials stability to the environmental gas.

3.2. Effect of Annealing Time on Battery Performance. To examine the effect of annealing duration before the battery test on its performance, we assembled two batteries, i.e., battery−(A) and battery−(B), and the former and latter batteries were kept in open circuit for 2 and 200 h, respectively, at 393 K. Then, the initial discharge was carried out at 0.1 C. Figure 3a shows the charge, Q, passing through the battery−

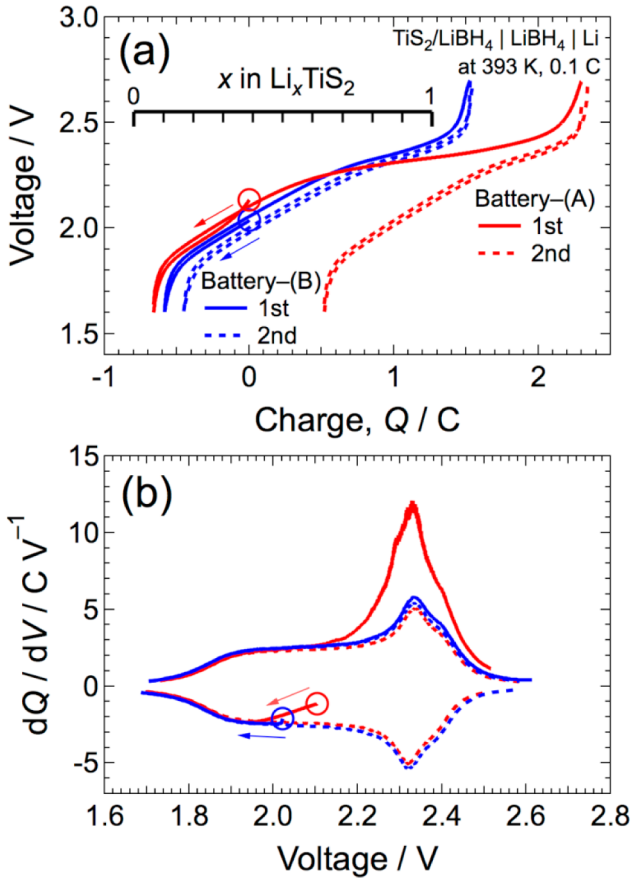

Figure 3. (a) Charge, Q, passing through the bulk-type all-solid-state TiS_2/Li batteries operated at 393 K and 0.1 C. The temperature was first raised up to 393 K, and subsequently the discharges were started after 2 and 200 h for battery−(A) and −(B), respectively. The discharges of battery−(A) and −(B) were started from red and blue circles, respectively. (b) dQ/dV-plot derived from the discharge−charge profiles of battery−(A) and −(B).

(A) and −(B) operated at 393 K and 0.1 C. Figure 3b shows the dQ/dV plot derived from the discharge−charge profiles of the batteries shown in Figure 3a.

The short time (2 h) annealed battery−(A) overcharged in the initial cycle for 0.9 coulomb, corresponding to $x \sim 0.45$ in Li_xTiS_2 at the upper cutoff voltage of 2.7 V. During the initial charge, an irreversible electrochemical oxidation wave attributed to the side-reaction appeared in the voltage range of ≥2.1 V, as evident in the dQ/dV-plot in Figure 3b. Such an irreversible electrochemical oxidation was not observed from the second cycle onward, and the Coulombic efficiency became almost 100%. On the other hand, the overcharge was less pronounced for the long time (200 h) annealed battery−(B). Both cells exhibited notable cycle stability. The capacity retention ratios of the 50th discharge to the second discharge for battery−(A) and −(B) were 99% and 93%, respectively, with almost 100% Coulombic efficiency over the battery test (data not shown).

In the nonaqueous system, the intercalation of Li from $LiBH_4$ into TiS_2, i.e., the self-discharge reaction, is proposed as[43]

DOI: 10.1021/acs.chemmater.5b02110
Chem. Mater. 2015, 27, 5407−5416

$$TiS_2 + xLiBH_4 \rightarrow Li_xTiS_2 + (x/2)B_2H_6 + (x/2)H_2 \quad (1)$$

The reaction 1 is the oxidation reaction of $LiBH_4$, and it would take place in the composite positive electrode layer during annealing before the initial discharge. Once $LiBH_4$ near TiS_2 in the composite positive electrode is oxidized during annealing and/or electrochemically oxidized during charging, the battery could be stably operated with nearly 100% Coulombic efficiency. This implies that the oxidation reaction of $LiBH_4$ at the interface with TiS_2 would be a factor determining the cycle life of the bulk-type all-solid-state TiS_2/Li battery.

To examine, in more detail, the effect of self-discharge owing to the solid-state reaction between TiS_2 and $LiBH_4$ on the battery performance, we carried out TG coupled with gas composition analysis using a QMS at elevated temperatures in He flow. Figure 4 shows the profiles of TG and H_2 and

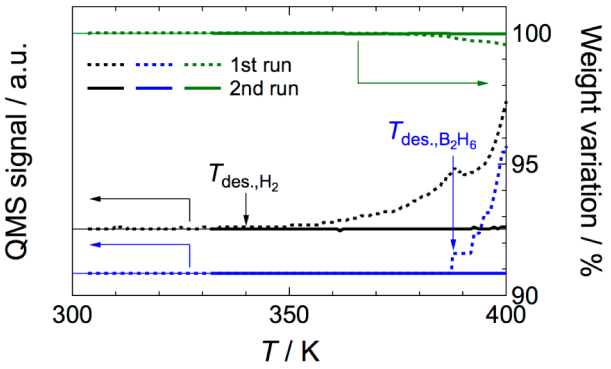

Figure 4. Profiles of TG (green curve) and H_2 (m/z = 2, black curve) and B_2H_6 (m/z = 27, blue curve) desorption from the TiS_2 and $LiBH_4$ composite at elevated temperatures in He flow. Broken and solid curves represent the profiles of the first and second heating runs, respectively.

diborane (B_2H_6) desorption from the compact consisting of TiS_2 and $LiBH_4$ at elevated temperatures. Desorption of H_2 and B_2H_6 takes place at 330 and 390 K, respectively, in the first heating run. Accompanied by the gas desorption, the weight of the mixed TiS_2 and $LiBH_4$ compact decreased by approximately 0.5% at 400 K. Such low-temperature gas desorption is unlikely to occur for the as-received $LiBH_4$. H_2 desorption from $LiBH_4$ generally occurs at temperatures higher than the melting temperature, i.e., 550 K.[8,44,45] This suggests that the low-temperature gas desorption seen in Figure 4 is a phenomenon specific to the TiS_2/$LiBH_4$ mixture accompanied by the solid-state reaction between them. It should be noted here that H_2 desorption starts at lower temperatures compared to B_2H_6. Diborane is considered as a byproduct of H_2 release during the thermal decomposition of $LiBH_4$. Actually, the H_2 and B_2H_6 desorption rates are independent of each other, and both depend on the surface structure of $LiBH_4$.[42] Thus, the existence of the intermediate compound in the thermal decomposition reaction of $LiBH_4$ is pronounced,[8,44−48] as discussed later. Weight variation of the TiS_2 and $LiBH_4$ compact started at temperatures lower than B_2H_6 desorption and around H_2 release. The major gas desorbed from $LiBH_4$ is thus H_2. Consequently, the reaction between TiS_2 and $LiBH_4$ may not be simply described by reaction 1. During the second heating run, no gas evolution or significant weight loss occurred, even though a large amount of unreacted $LiBH_4$ was still present in the specimen. This suggests that the chemical reaction that accompanies gas desorption is limited to the very beginning of the annealing process, presumably from areas adjacent to the interface between $LiBH_4$ and TiS_2 in the composite.

Due to the self-discharge reaction that accompanies the gas desorption, $LiBH_4$ just beneath the TiS_2 surface is oxidized. This trend is consistent with the situation observed by the electrochemical measurements as discussed earlier in this section. That is, when the solid-state reaction is not finished owing to an insufficient annealing duration, the electrochemical irreversible oxidation takes place in the initial charge. This means that the oxidation reaction of $LiBH_4$ plays an essential role in the formation of the stable interface that hinders the solid-state reaction between TiS_2 and $LiBH_4$ and allows for the repeated discharge−charge cycles.

Thermal decomposition of $LiBH_4$ proceeds by a stepwise reaction pathway that includes lithium dodecahydro-*closo*-dodecaborate, $Li_2B_{12}H_{12}$, as an intermediate phase:[8,44−48]

$$LiBH_4 \rightarrow (1/12)Li_2B_{12}H_{12} + 5/6LiH + 13/12H_2$$
$$\rightarrow LiH + B + (3/2)H_2 \quad (2)$$

Orimo and co-workers experimentally observed the formation of $Li_2B_{12}H_{12}$ as a result of thermal decomposition of $LiBH_4$.[46] Ohba and co-workers have examined the phase relationship of the ternary Li−B−H−hydrides by the first-principles calculations. The authors suggested that $Li_2B_{12}H_{12}$ is thermodynamically stable and thereby occurs as an intermediate phase during the course of H_2 release from $LiBH_4$.[47] Since the major gas desorbed from $LiBH_4$ just beneath the TiS_2 surface is H_2, the solid-state reaction between TiS_2 and $LiBH_4$ most likely forms $Li_2B_{12}H_{12}$ at their interface.

3.3. Chemical Reactivity between TiS_2 and $LiBH_4$.

As emphasized in the previous section, oxidation of $LiBH_4$ plays an important role in the formation of the stable interface that allows repeated discharge−charge cycles of the bulk-type all-solid-state TiS_2/Li battery. Self-discharge, i.e., Li intercalation into TiS_2 by reaction 1, should accompany the lattice expansion of TiS_2. Thus, we examined here the solid-state reactivity between TiS_2 and $LiBH_4$ by means of powder XRD measurements.

Figure 5a compares the XRD patterns of the as-received $LiBH_4$, TiS_2, and the TiS_2 and $LiBH_4$ mixture annealed at 393 K for 2 h in an Ar-filled environment. It is obvious that the diffraction peaks from TiS_2 shifted toward lower angle after annealing. This means that lattice expansion of TiS_2 occurs by mixing with $LiBH_4$ and subsequent annealing at high temperatures. The as-received TiS_2 (space group: $P\bar{3}m1$) had the lattice parameters of a = 0.34061(2) nm and c = 0.56986(7) nm. These are consistent with the literature data of a = 0.34079(3) nm and c = 0.56989(6) nm.[38,39] From the XRD patterns shown in Figure 5a, the lattice parameters of TiS_2 as a result of annealing at 393 K for 2 h were a = 0.34392(2) nm and c = 0.61917(4) nm.

Dahn and Haering systematically investigated the lattice parameters of Li_xTiS_2 as a function of x.[38,39] By comparing their data with the lattice parameters of TiS_2 after annealing with $LiBH_4$, the Li concentration, x, in Li_xTiS_2 was estimated under the assumption that the lattice expansion of TiS_2 was caused only by the Li intercalation from $LiBH_4$ into TiS_2, i.e., a self-discharge reaction. The Li concentration as a result of annealing was 0.67, corresponding to the specific capacity of ∼160 mAh g^{-1}. The specific capacity owing to the self-discharge reaction is close to the difference between the theoretical capacity and the

DOI: 10.1021/acs.chemmater.5b02110
Chem. Mater. 2015, 27, 5407−5416

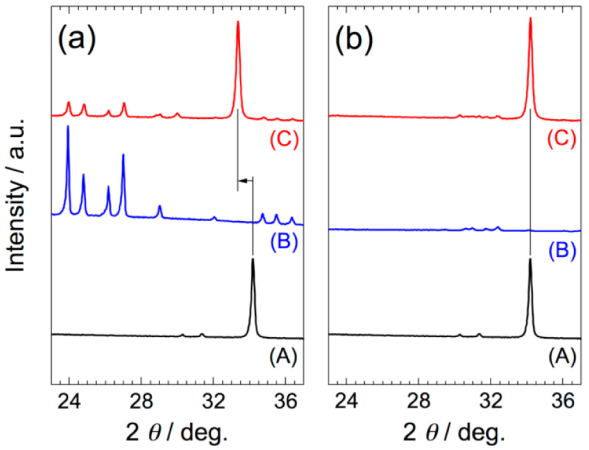

Figure 5. Room temperature XRD patterns: (a) (A) as-received $LiBH_4$ (space group: *Pnma*),[49] (B) as-received TiS_2 (space group: $P\bar{3}m1$),[38,39] and (C) the TiS_2 and $LiBH_4$ mixture (weight ratio: w_{TiS2}:w_{LiBH4} = 2:3, and molar ratio: m_{Li}/m_{Ti} = 7.7) after annealing at 393 K for 2 h in an Ar-filled environment. (b) (A) as-prepared $Li_2B_{12}H_{12}$ (space group: $Pa\bar{3}$),[32] (B) as-received TiS_2, and (C) the TiS_2 and $Li_2B_{12}H_{12}$ mixture (weight ratio: w_{TiS2}:$w_{Li2B12H12}$ = 2:3, and molar ratio: m_{Li}/m_{Ti} = 2.2) after annealing at 393 K for 2 h in an Ar-filled environment.

initial discharge capacity of ~150 mAh g^{-1}, as shown in Figure 2a.[19] It should be noted here that the Li concentration, *x*, in Li_xTiS_2 increased by increasing the annealing time and/or the molar ratio of Li to Ti, m_{Li}/m_{Ti}, in the TiS_2/$LiBH_4$ mixture (see details in Supporting Information, Figure S4 and Table S1). We hypothesize that only lithium borohydride just beneath the TiS_2 surface contributes to the solid-state reaction between TiS_2 and $LiBH_4$. The result is consistent with the microstructure observation of the TiS_2 and $LiBH_4$ compact after annealing. That is, the microstructure change owing to the solid-state reaction between $LiBH_4$ and TiS_2 is roughly limited to the $LiBH_4$ phase just beneath the edge-plane of TiS_2, as displayed in Supporting Information Figure S1.

3.4. Electrochemical Response of Crystalline $Li_2B_{12}H_{12}$. To see whether $Li_2B_{12}H_{12}$ can act as a battery electrolyte, the lithium-ionic conductivity and charge transfer reactivity of crystalline $Li_2B_{12}H_{12}$ for lithium ions were examined using Li- and Au-symmetric cells at 393 K by means of the two-probe ac technique. Figure 6a compares the ac impedance spectra of the Li- and Au-symmetric cells using the crystalline $Li_2B_{12}H_{12}$ electrolyte at 393 K. For the Li-symmetric cell, only a semicircle appeared in a complex plane. On the other hand, the Au-symmetric cell had the series of a semicircle and a spike in the high and low frequency regions, respectively. The results suggest that the Au electrode forms a blocking interface while the Li electrode forms a reversible interface with the $Li_2B_{12}H_{12}$ electrolyte. The semicircle appearing for both symmetric cells represents the electrolyte resistance, and the lithium ionic conductivity was calculated to be $\log(\sigma / S\ cm^{-1}) = -4.4$ at 393 K.

The lithium ionic conductivity of $Li_2B_{12}H_{12}$ is lower than that of $LiBH_4$ by approximately 2 orders of magnitude. Since the reaction (precipitation of $Li_2B_{12}H_{12}$) would be limited to just beneath the TiS_2 surface, such a precipitation of the intermediate layer that has lower lithium ionic conductivity does not significantly affect the total battery resistance. Our composite positive electrode contains excess $LiBH_4$ against TiS_2, and approximately 10 mol % $LiBH_4$ (at maximum by assuming full Li intercalation in TiS_2 to form $LiTiS_2$) can

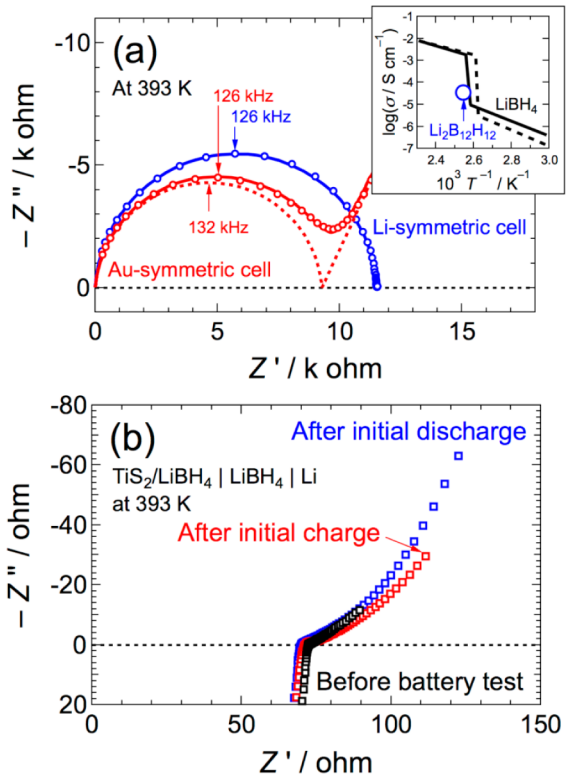

Figure 6. AC impedance spectra. (a) Li- and Au-symmetric cells using the crystalline $Li_2B_{12}H_{12}$ electrolyte at 393 K. The electrolyte thicknesses of 1.9 and 1.75 mm were used for Li- and Au-symmetric cells, respectively. (b) Bulk-type all-solid-state TiS_2/Li battery just before the battery test (black) and after first discharge (blue) and first charge (red) at 393 K.

contribute to the self-discharge reaction. Figure 6b compares the ac impedance spectra of the bulk-type all-solid-state TiS_2/Li battery just before the battery test and after the first discharge and charge at 393 K. The electrolyte resistance derived by the ohmic resistance was $\log(\sigma / S\ cm^{-1}) = -2.8$ regardless of the Li_xTiS_2 composition. This value fairly agrees with the lithium ionic conductivity of $LiBH_4$.[17] This implies that the established interface layer including $Li_2B_{12}H_{12}$ (with its lower lithium ionic conductivity) does not contribute to the total resistance owing to its limited thickness in the composite positive electrode in our battery configuration.

3.5. Chemical Reactivity between TiS_2 and $Li_2B_{12}H_{12}$. Contrary to the TiS_2 and $LiBH_4$ mixture, the lattice expansion of TiS_2 was not observed for the TiS_2 and $Li_2B_{12}H_{12}$ mixture as a result of annealing at 393 K for 2 h as shown in Figure 5b. This suggests that crystalline $Li_2B_{12}H_{12}$ has higher oxidative stability than $LiBH_4$, and thereby the solid-state reaction between $Li_2B_{12}H_{12}$ and TiS_2 is hindered. In addition, $Li_2B_{12}H_{12}$ has a lithium ionic conductivity of $\log(\sigma/S\ cm^{-1}) = -4.4$ and charge transfer reactivity with the Li-electrode. Considering the above, $Li_2B_{12}H_{12}$ would act as a stable interface layer that allows repeated discharge−charge cycles without any remarkable side reaction or self-discharge.

3.6. Evaluation of Equilibrium Potentials of Constituents of the Bulk-Type All-Solid-State TiS_2/Li Battery. FPMD calculations were performed to better understand and quantitatively evaluate the electrochemical stabilities of the interfaces of TiS_2 with $LiBH_4$ and $Li_2B_{12}H_{12}$. Spectroscopic techniques did not identify the products formed by solid-state

DOI: 10.1021/acs.chemmater.5b02110
Chem. Mater. 2015, 27, 5407−5416

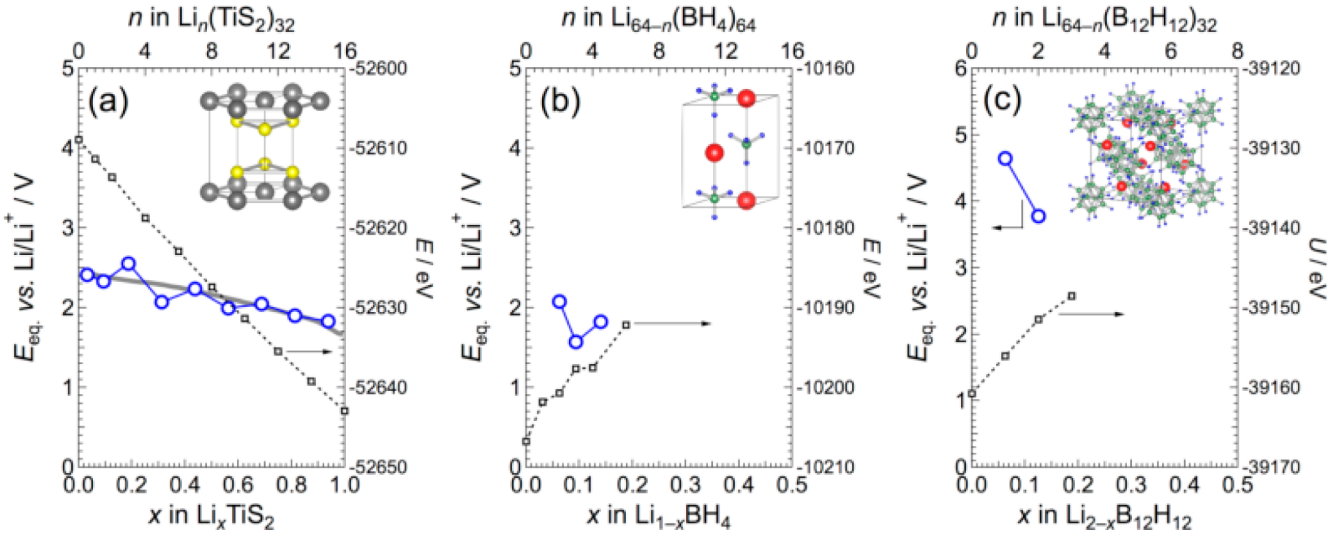

Figure 7. Equilibrium potentials, E_{eq} (vs Li/Li$^+$), and internal energies, U, of (a) Li_xTiS_2, (b) $Li_{1-x}BH_4$, and (c) $Li_{2-x}B_{12}H_{12}$ as a function of the lithium concentration, x, in the compounds at 410 K. Zero energy of U is arbitrarily set. Gray curve in (a) shows the OCP of Li_xTiS_2 evaluated by the Coulombic titration technique using the bulk-type all-solid-state TiS_2/Li battery at 393 K. Only relative values in U are used.

reaction at the interface between TiS_2 and $LiBH_4$, probably owing to their small concentration in the composite. Although it is known that complex hydrides with polyhedral anions have high oxidative stability in nonaqueous systems,[50] the electrochemical stability of the salt itself is not clarified. Therefore, we used FPMD simulations to predict the materials stability at the interface. The equilibrium potential, E_{eq}, of the Li containing species, Li_nM, at the charge transfer interface is expressed as

$$Li_nM + Li^+ + e^- = Li_{n+1}M \quad (3)$$

E_{eq} of Li_xTiS_2 as a function of x is measurable by the electrochemical technique, and those of the electrolytes like $LiBH_4$ and $Li_2B_{12}H_{12}$ are not. It is possible to calculate them by introducing $Li = Li^+ + e^-$, in equilibrium 3, resulting in,

$$Li_nM + Li = Li_{n+1}M \quad (4)$$

E_{eq} of equilibrium 3 is related to the Gibbs free energy change, ΔG, i.e., $E_{eq}F = -\Delta G$, where F is the Faraday constant. Since free energy is not easily calculated from first-principles because of the entropic term, internal energy was obtained from total energy in the FPMD calculations at a certain temperature. Internal energy of the system including Li is introduced as $U(Li_nM) = U_{total}(Li_nM) - nU_{total}(Li)$, and for the equilibrium, $Li_nM + Li = Li_{n+1}M$. Each term is the time-average total energy of the individual system. E_{eq} of the constituents, Li_nM (M = TiS_2, BH_4, and $B_{12}H_{12}$), were derived by taking the slope of the internal energy as a function of number of Li, n. That is,

$$E_{eq.}F = -dU(Li_nM)/dn \quad (5)$$

Figure 7a–c shows the equilibrium potentials, E_{eq}, as a function of x in Li_xTiS_2, $Li_{1-x}BH_4$, and $Li_{2-x}B_{12}H_{12}$, respectively, at 410 K. In these figures, x was converted from the Li number, n, in the individual supercell (see details on the models and calculation conditions for the FPMD in Supporting Information, Table S2). The gray curve in Figure 7a shows the OCP that was experimentally evaluated by the Coulombic titration method by using the bulk-type all-solid-state TiS_2/Li battery at 393 K. Calculated $E_{eq} \sim 2.5$ of TiS_2 agrees well with the experimentally obtained OCP (see details of the OCP measurements in Supporting Information, Figure S5). When Li atoms are removed from $LiBH_4$, the BH_4 unit is decomposed to give various B–H chemical species including BH_3, BH_5, B_2H_7, and B_2H_6. BH_5 has four sp^3 bonds, one of which is a bond with H_2. B_2H_7 has an H atom shared by the two BH_3 units. The intermediates including BH_3, BH_5, and BH_7 are unstable and decompose into stable B_2H_6 and H_2 molecules. B_2H_6 is a known byproduct of H_2 release during the decomposition of $LiBH_4$.[42] This is consistent with the observation that H_2 and B_2H_6 were released from the composite containing TiS_2 and $LiBH_4$ in the first heating run of the TG coupled with QMS analysis, as shown in Figure 4.

$Li_{1-x}BH_4$ and $Li_{2-x}B_{12}H_{12}$ have E_{eq} of 1.6–2.1 V and >4.0 V (vs Li/Li$^+$), respectively, at $x \leq 0.1$. The lithium transfer reaction likely occurs from $LiBH_4$ into TiS_2 since $LiBH_4$ has a lower E_{eq} than TiS_2. This Li intercalation was experimentally confirmed by a lattice expansion by means of the powder XRD measurements, as shown in Figure 5a. In the TG coupled with QMS analysis at elevated temperatures, we observed H_2 and B_2H_6 release from the TiS_2 and $LiBH_4$ mixture owing to the solid-state reaction between them, as shown in Figure 4. These results agree with the FPMD simulation results. The low-voltage $Li_4Ti_5O_{12}$ allows the operation of the solid-state battery for repeated cycles without any protection layer between $Li_4Ti_5O_{12}$ and the complex hydride electrolyte,[23] contrary to the high-voltage $LiCoO_2$ positive electrode.[21,22] This is also consistent with the FPMD simulation result on $LiBH_4$. E_{eq} of $LiTiS_2$ remains still as high as ~1.8 V, meaning that the FPMD simulation result predicts the Li intercalation into TiS_2 to form $LiTiS_2$. Although our composite positive electrode contains an approximately 10-fold (in mol %) excess $LiBH_4$ with respect to TiS_2, x in Li_xTiS_2 was only 0.67 as the result of the solid-state reaction between TiS_2 and $LiBH_4$. The suppression of the reaction is not a thermodynamic issue but is owing to the formation of the interface that hinders the reaction between TiS_2 and $LiBH_4$. $Li_2B_{12}H_{12}$ has higher redox potential than TiS_2, and thereby the solid-state reaction between them does not take place. This is consistent with the result of the powder XRD measurements in Figure 5b that no lattice expansion of TiS_2 owing to Li intercalation occurs for the TiS_2 and $Li_2B_{12}H_{12}$ composite. Since $Li_2B_{12}H_{12}$ has a lithium ionic conductivity of

DOI: 10.1021/acs.chemmater.5b02110
Chem. Mater. 2015, 27, 5407–5416

$\log(\sigma / S\ cm^{-1}) = -4.4$ at 393 K and allows the charge transfer of Li ions with the electrode, the $Li_2B_{12}H_{12}$ would act as a stable interface that allows the repeated battery operation (similar to the SEI forming between the nonaqueous electrolyte and graphite negative electrode)[29] as the discharge−charge profiles shown in Figure 2a.

The results shown here could provide the design principles of bulk-type all-solid-state batteries: (1) In addition to TiS_2 as examined in this study, elemental sulfur, which has a high theoretical capacity (1672 mAh g^{-1}) with a redox potential of ~2.2 V,[28] is advantageous to realize long cycle life. Since the reductive decompositions of elemental sulfur are unlikely occur at the interface with complex hydride electrolytes, the interface formed among them may also contribute to stable battery operation. Actually, we realized repeated discharge−charge cycles with high sulfur utilization ratio by using the $LiBH_4$-based electrolyte.[24,25] (2) Closo-borane hydrides, including $Na_2B_{12}H_{12}$ and $Na_2B_{10}H_{10}$ that we recently discovered to exhibit fast Na-ionic conduction, would be also beneficial to be incorporated into bulk-type all-solid-state batteries. In these materials, quick reorientational motion of the complex anion, including $[B_{12}H_{12}]^{2-}$ and $[B_{10}H_{10}]^{2-}$, assist the mobility of ionic carriers and enable the formation of ion transport channels in the crystal latice,[51,52] similar to the high-temperature phase of $LiBH_4$.[53−55] This class of materials will form stable interfaces with the various positive electrodes without any interface microstructure changes (see Supporting Information Figure S1) owing to their high oxidative stability and thereby allow for longer-cycle-life battery operation.

4. CONCLUSION

In this study, we successfully realized 300 discharge−charge cycles for the bulk-type all-solid-state TiS_2/Li battery using a $LiBH_4$ electrolyte at 393 K and 0.2 C. Our battery exhibited a second discharge capacity of 205 mAh g^{-1}, corresponding to a TiS_2 utilization ratio of 85%. Our battery also exhibited a high capacity retention ratio of 88% at the 300th discharge (compared to the second discharge) with nearly 100% Coulombic efficiency from the second cycle. The effect of exposure of $LiBH_4$ to atmospheric-pressure oxygen on the battery performance was less pronounced. To examine the origin of the cycle stability of our battery, we carried out electrochemical measurements, TG coupled with gas composition analysis, powder XRD measurements, and FPMD simulations. The chemical and/or electrochemical oxidation of $LiBH_4$ took place just beneath the TiS_2 surface at the battery operating temperature of 393 K before the initial discharge and/or during the initial charge. The process is accompanied by H_2 desorption from $LiBH_4$ and leads to a composition variation for $LiBH_4$ adjacent to the TiS_2 surface. $Li_2B_{12}H_{12}$ is the likely product of $LiBH_4$ oxidation, as it has sufficient oxidative stability to act as a protective surface layer to hinder further chemical reactions between the borohydride and TiS_2 species. It exhibits a lithium ionic conductivity of $\log(\sigma / S\ cm^{-1}) = -4.4$ at 393 K and a charge transfer reactivity with the Li-electrode and thereby can act as the robust interface layer that allows for the numerous discharge−charge cycles observed. Our experiments and calculations suggest that the stable interface formation mechanism is likely a direct consequence of the existence of highly inert, hydrogen-deficient complex hydrides such as $Li_2B_{12}H_{12}$ within the Li−B−H ternary system. Future experiments are planned to further probe the formation, extent, and chemical composition of this robust interface layer via a combination of carefully tailored, flat TiS_2/$LiBH_4$ thin-film specimens and neutron reflectometry.[56]

■ ASSOCIATED CONTENT

Supporting Information

Experimental results on the reactivity between TiS_2 and Li−B−H complex hydrides, Coulombic titration, and battery tests and details on FPMD simulations. The Supporting Information is available free of charge on the ACS Publications website at DOI: 10.1021/acs.chemmater.5b02110.

■ AUTHOR INFORMATION

Corresponding Author

*(A.U.) E-mail: unemoto@imr.tohoku.ac.jp.

Author Contributions

The manuscript was written through contributions of all authors.

Notes

The authors declare no competing financial interest.

■ ACKNOWLEDGMENTS

The crystal structures in Figure 7 were drawn using the VESTA program.[57] The authors would like to thank Mr. K. Sato, Ms. H. Ohmiya, and Ms. N. Warifune for technical assistances. Fruitful discussion with Mr. G. Nogami, Mr. M. Tazawa, and Dr. M. Taniguchi of Mitsubishi Gas Chemicals Co., Ltd., is also acknowledged. This work was partially supported by the Target Project 4 of WPI−AIMR, Tohoku University, the Integrated Materials Research Center for the Low-Carbon Society (LC−IMR), Tohoku University, JSPS KAKENHI Grant No. 25220911, the Advanced Low Carbon Technology Research and Development Program (ALCA) from the Japan Science and Technology Agency, and the U.S. Department of Energy (DOE) Office of Energy Efficiency and Renewable Energy under Grant No. DE-EE0002978. The FPMD calculations have been performed under the interuniversity cooperative research program of the Center for Computational Materials Science, Institute for Materials Research, Tohoku University. The battery assembly in a dry room was carried out at NIMS Battery Research Platform, Tsukuba, Japan.

■ REFERENCES

(1) Goodenough, J. B.; Park, K.−S. The Li-ion rechargeable battery: A perspective. *J. Am. Chem. Soc.* **2013**, *135*, 1167−1176.
(2) Takada, K. Progress and prospective of solid-state lithium batteries. *Acta Mater.* **2013**, *61*, 759−770.
(3) Kato, Y.; Kawamoto, K.; Kanno, R.; Hirayama, M. Discharge performance of all-solid-state battery using a lithium superionic conductor $Li_{10}GeP_2S_{12}$. *Electrochemistry* **2012**, *80*, 749−751.
(4) Kamaya, N.; Homma, K.; Yamakawa, Y.; Hirayama, M.; Kanno, R.; Yonemura, M.; Kamiyama, T.; Kato, Y.; Hama, S.; Kawamoto, K.; Mitsui, A. A lithium superionic conductor. *Nat. Mater.* **2011**, *10*, 682−686.
(5) Sakuda, A.; Hayashi, A.; Tatsumisago, M. Interfacial observation between $LiCoO_2$ electrode and Li_2S−P_2S_5 solid electrolytes of all-solid-state lithium secondary batteries using transmission electron microscopy. *Chem. Mater.* **2010**, *22*, 949−956.
(6) Brazier, A.; Dupont, L.; Dantras-Laffont, L.; Kuwata, N.; Kawamura, J.; Tarascon, J.−M. First cross-section observation of an all solid-state lithium-ion "nanobattery" by transmission electron microscopy. *Chem. Mater.* **2008**, *20*, 2352−2359.
(7) Schlapbach, L.; Züttel, A. Hydrogen-storage materials for mobile applications. *Nature* **2001**, *414*, 353−358.

DOI: 10.1021/acs.chemmater.5b02110
Chem. Mater. 2015, 27, 5407−5416

(8) Orimo, S.; Nakamori, Y.; Eliseo, J. R.; Züttel, A.; Jensen, C. M. Complex hydrides for hydrogen storage. *Chem. Rev.* **2007**, *107*, 4111−4132.
(9) Oumellal, Y.; Rougier, A.; Nazri, G. A.; Tarascon, J.−M.; Aymard, L. Metal hydrides for lithium-ion batteries. *Nat. Mater.* **2008**, *7*, 916−921.
(10) Zaïdi, W.; Oumellal, Y.; Bonnet, J.−P.; Zhang, J.; Cuevas, F.; Latroche, M.; Bobet, J.−L.; Aymard, L. Carboxymethylcellulose and carboxymethylcellulose-formate as binders in MgH_2-carbon composites negative electrode for lithium-ion batteries. *J. Power Sources* **2011**, *196*, 2854−2857.
(11) Oumellal, Y.; Courty, M.; Rougier, A.; Nazri, G. A.; Aymard, L. Electrochemical reactivity of magnesium hydride toward lithium: New sysnthesis route of nano-particles suitable for hydrogen storage. *Int. J. Hydrogen Energy* **2014**, *39*, 5852−5857.
(12) Oumellal, Y.; Zlotea, C.; Bastide, S.; Cachet-Vivier, C.; Leonel, E.; Sengmany, S.; Leroy, E.; Aymard, L.; Bonnet, J.−P.; Latroche, M. Bottom-up preparation of MgH_2 nanoparticles with enhanced cycle life stability during electrochemical conversion in Li-ion batteries. *Nanoscale* **2014**, *6*, 14459−14466.
(13) Wietelmann, U. Applications of lithium-containing hydrides for energy storage and conversion. *Chem. Ing. Tech.* **2014**, *86*, 2190−2194.
(14) Zaïdi, W.; Bonnet, J.−P.; Zhang, J.; Cuevas, F.; Latroche, M.; Couillaud, S.; Bobet, J.−L.; Sougrati, M. T.; Jumas, J.−C.; Aymard, L. Reactivity of complex hydrides Mg_2FeH_6, Mg_2CoH_5 and Mg_2NiH_4 with lithium ion: Far from equilibrium electrochemically driven conversion reactions. *Int. J. Hydrogen Energy* **2013**, *38*, 4798−4808.
(15) Zhang, J.; Zaïdi, W.; Paul-Boncour, V.; Provost, K.; Michalowicz, A.; Cuevas, F.; Latroche, M.; Belin, S.; Bonnet, J.−P.; Aymard, L. XAS investigations on nanocrystalline Mg_2FeH_6 used as a negative electrode of Li-ion batteries. *J. Mater. Chem. A* **2013**, *1*, 4706−4717.
(16) Dahn, J.; Zheng, T.; Liu, Y.; Xue, J. S. Mechanisms for lithium insertion in carbonaceous materials. *Science* **1995**, *270*, 590−593.
(17) Matsuo, M.; Nakamori, Y.; Orimo, S.; Maekawa, H.; Takamura, H. Lithium superionic conduction in lithium borohydride accompanied by structure transition. *Appl. Phys. Lett.* **2007**, *91*, 224103.
(18) Matsuo, M.; Orimo, S. Lithium fast-ionic conduction in complex hydrides: Review and prospects. *Adv. Energy Mater.* **2011**, *1*, 161−172.
(19) Unemoto, A.; Matsuo, M.; Orimo, S. Complex hydrides for electrochemical energy storage. *Adv. Funct. Mater.* **2014**, *24*, 2267−2279.
(20) Maekawa, H.; Matsuo, M.; Takamura, H.; Ando, M.; Noda, Y.; Karahashi, T.; Orimo, S. Halide-stabilized $LiBH_4$, a room-temperature lithium fast-ion conductor. *J. Am. Chem. Soc.* **2009**, *131*, 894−895.
(21) Takahashi, K.; Hattori, K.; Yamazaki, T.; Takada, K.; Matsuo, M.; Orimo, S.; Maekawa, H.; Takamura, H. All-solid-state lithium battery with $LiBH_4$ solid electrolyte. *J. Power Sources* **2013**, *226*, 61−64.
(22) Takahashi, K.; Maekawa, H.; Takamura, H. Effects of intermediate layer on interfacial resistance for all-solid-state lithium batteries using lithium borohydride. *Solid State Ionics* **2014**, *262*, 179−182.
(23) Sveinbjörnsson, D.; Christiansen, A. S.; Viskinde, R.; Norby, P.; Vegge, T. The $LiBH_4$-LiI solid solution as an electrolyte in an all-solid-state battery. *J. Electrochem. Soc.* **2014**, *161*, A1432−A1439.
(24) Unemoto, A.; Yasaku, S.; Nogami, G.; Tazawa, M.; Taniguchi, M.; Matsuo, M.; Ikeshoji, T.; Orimo, S. Development of bulk-type all-solid-state lithium-sulfur battery using $LiBH_4$ electrolyte. *Appl. Phys. Lett.* **2014**, *105*, 083901.
(25) Unemoto, A.; Chen, C.; Wang, Z.; Matsuo, M.; Ikeshoji, T.; Orimo, S. Pseudo-binary electrolyte, $LiBH_4$−LiCl, for bulk-type all-solid-state lithium-sulfur batter. *Nanotechnology* **2015**, *26*, 254001.
(26) Ohzuku, T.; Ueda, A. Solid-state redox reactions of $LiCoO_2$ (R−3m) for 4 V secondary lithium cells. *J. Electrochem. Soc.* **1994**, *141*, 2972−2977.
(27) Takada, K.; Aotani, N.; Iwamoto, K.; Kondo, S. Solid state lithium battery with oxysulfide glass. *Solid State Ionics* **1996**, *86*−*88*, 877−882.
(28) Bruce, P. G.; Freunberger, S. A.; Hardwick, L. J.; Tarascon, J.−M. Li-O_2 and Li-S batteries with high energy storage. *Nat. Mater.* **2012**, *11*, 19−29.
(29) Peled, E. The electrochemical behavior of alkali and alkaline earth metals in nonaqueous battery systems−The solid electrolyte interphase mode. *J. Electrochem. Soc.* **1979**, *126*, 2047−2051.
(30) The mention of all commercial suppliers in this paper is for clarity and does not imply the recommendation or endorsement of these suppliers by NIST.
(31) Johnson, J. W.; Brody, J. F. Lithium closoborane electrolytes III. Preparation and characterization. *J. Electrochem. Soc.* **1982**, *129*, 2213−2219.
(32) Her, J.−H.; Yousufuddin, M.; Zhou, W.; Salisatgi, S. S.; Kulleck, J. G.; Zhan, J. A.; Hwang, S.−J.; Bowman, R. C., Jr.; Udovic, T. J. Crystal structure of $Li_2B_{12}H_{12}$: a possible intermediate species in the decomposition of $LiBH_4$. *Inorg. Chem.* **2008**, *47*, 9757−9759.
(33) Vanderbilt, D. Soft self-consistent pseudopotentials in a generalized eigenvalue formalism. *Phys. Rev. B: Condens. Matter Mater. Phys.* **1990**, *41*, 7892−7895.
(34) Perdew, J. P.; Burke, K.; Ernzerhof, M. Generalized gradient approximation made simple. *Phys. Rev. Lett.* **1996**, *77*, 3865−3868.
(35) Morikawa, Y.; Iwata, K.; Terakura, T. Theoretical study of hydrogeneration process of formate on clean and Zn deposited Cu(111) surfaces. *Appl. Surf. Sci.* **2001**, *169*−*170*, 11−15.
(36) Whittingham, M. S. Electrical energy storage and intercalation chemistry. *Science* **1976**, *192*, 1126−1127.
(37) Whittingham, M. S. Chemistry of intercalation compounds: metal guests in chalcogenide hosts. *Prog. Solid State Chem.* **1978**, *12*, 41−99.
(38) Dahn, J.; Haering, R. R. Anomalous bragg peak width in Li_xTiS_2. *Solid State Commun.* **1981**, *40*, 245−248.
(39) Dahn, J.; McKinnon, W.; Haering, R. R.; Buyers, W.; Powell, B. Structure determination of Li_xTiS_2 by neutron diffraction. *Can. J. Phys.* **1980**, *58*, 207−213.
(40) Schlesinger, H. I.; Brown, H. C.; Finholt, A. E.; Gilbreath, J. R.; Hoekstra, H. R.; Hyde, E. K. Sodium borohydride, its hydrolysis and its use as a reducing agent and in the generation of hydrogen. *J. Am. Chem. Soc.* **1953**, *75*, 215−219.
(41) Kojima, Y.; Kawai, Y.; Kimbara, M.; Nakanishi, H.; Matsumoto, S. Hydrogen generation by hydrolysis reaction of lithium borohydride. *Int. J. Hydrogen Energy* **2004**, *29*, 1213−1217.
(42) Kato, S.; Bielmann, M.; Borgschulte, A.; Zakaznova-Herzog, V.; Remhof, A.; Orimo, S.; Züttel, A. Effect of the surface oxidation of $LiBH_4$ on the hydrogen desorption mechanism. *Phys. Chem. Chem. Phys.* **2010**, *12*, 10950−10955.
(43) Kanatzidis, M. G.; Marks, T. J. Tetrahydroborate intercalation reagents. Convenient, straightforward routes to known and new types of layered intercalation compounds. *Inorg. Chem.* **1987**, *26*, 783−784.
(44) Züttel, A.; Rentsch, S.; Fischer, P.; Wenger, P.; Sudan, P.; Mauron, Ph.; Emmenegger, Ch. Mauron, Ph.; Emmengger, Ch. Hydrogen storage properties of $LiBH_4$. *J. Alloys Compd.* **2003**, *356*−*357*, 515−520.
(45) Pitt, M. P.; Paskevicius, M.; Brown, D. H.; Sheppard, D. A.; Buckley, C. E. Thermal stability of $Li_2B_{12}H_{12}$ and its role in the decomposition of $LiBH_4$. *J. Am. Chem. Soc.* **2013**, *135*, 6930−6941.
(46) Orimo, S.; Nakamori, Y.; Ohba, N.; Miwa, K.; Towata, S.; Züttel, A.; Aoki, M. Experimental studies on intermediate compounds of $LiBH_4$. *Appl. Phys. Lett.* **2006**, *89*, 021920.
(47) Ohba, N.; Miwa, K.; Aoki, M.; Noritake, T.; Towata, S.; Nakamori, Y.; Orimo, S.; Züttel, A. First-principles study on the stability of intermediate compounds of $LiBH_4$. *Phys. Rev. B: Condens. Matter Mater. Phys.* **2006**, *74*, 075110.
(48) Ozolins, V.; Majzoub, E. H.; Wolverton, C. First-principles prediction of thermodynamically reversible hydrogen storage reactions in the Li-Mg-Ca-B-H system. *J. Am. Chem. Soc.* **2009**, *131*, 230−237.
(49) Soulie, J., Ph.; Genaudin, G.; Cerny, R.; Yvon, K. Lithium boro-hydride $LiBH_4$ I. Crystal structure. *J. Alloys Compd.* **2002**, *346*, 200−205.

DOI: 10.1021/acs.chemmater.5b02110
Chem. Mater. 2015, 27, 5407−5416

(50) Morris, J. H.; Gysling, H. J.; Reed, D. Electrochemistry of boron compounds. *Chem. Rev.* **1985**, *85*, 51−76.
(51) Udovic, T. J.; Matsuo, M.; Unemoto, A.; Verdal, N.; Stavila, V.; Skripov, A. V.; Rush, J. J.; Takamura, H.; Orimo, S. Sodium superionic conduction in $Na_2B_{12}H_{12}$. *Chem. Commun.* **2014**, *50*, 3750−3752.
(52) Udovic, T. J.; Matsuo, M.; Tang, W. S.; Wu, H.; Stavila, V.; Soloninin, A. V.; Skoryunov, R. V.; Babanova, O. A.; Skripov, A. V.; Rush, J. J.; Unemoto, A.; Takamura, H.; Orimo, S. Exceptional superionic conductivity in disordered sodium decahydro-*closo*-decaborate. *Adv. Mater.* **2014**, *26*, 7622−7626.
(53) Ikeshoji, T.; Tsuchida, E.; Ikeda, K.; Matsuo, M.; Li, J.−W.; Kawazoe, Y.; Orimo, S. Diffuse and doubly split atom occupation in hexagonal $LiBH_4$. *Appl. Phys. Lett.* **2009**, *95*, 221901.
(54) Ikeshoji, T.; Tsuchida, E.; Morishita, T.; Ikeda, K.; Matsuo, M.; Kawazoe, Y.; Orimo, S. Fast-ionic conductivity of Li^+ in $LiBH_4$. *Phys. Rev. B: Condens. Matter Mater. Phys.* **2011**, *83*, 144301.
(55) Myrdal, J. S. G.; Blanchard, D.; Sveinbjörnsson, D.; Vegge, T. Li-ion conduction in the $LiBH_4$:LiI system from density functional theory calculations and quasi-elastic neutron scattering. *J. Phys. Chem. C* **2013**, *117*, 9084−9091.
(56) Dura, J. A.; Kelly, S. T.; Kienzle, P. A.; Her, J.−H.; Udovic, T. J.; Majkrzak, C. F.; Chung, C.−J.; Clemens, B. M. Porous Mg formation upon dehydrogeneration of MgH_2 thin films. *J. Appl. Phys.* **2011**, *109*, 093501.
(57) Momma, K.; Izumi, F. *Commission on Crystallogr. Comput., IUCr Newslett.* **2006***7*, 106−119.

DOI: 10.1021/acs.chemmater.5b02110
Chem. Mater. 2015, 27, 5407−5416